Progress In Electromagnetics Research, Vol. 116, 533–551, 2011

MULTI-CHANNEL SPCMB-TOPS SAR FOR HIGH-RESOLUTION WIDE-SWATH IMAGING

W. Xu[1, *], P. P. Huang[2], and Y. K. Deng[1]

[1]Department of Spaceborne Microwave Remote Sensing, Institute of Electronics, Chinese Academy of Sciences (IECAS), Beijing, China

[2]College of Information Engineering, Inner Mongolia University of Technology, Hohhot, Inner Mongolia, China

Abstract—To improve the impaired azimuth resolution of the novel Terrain Observation by Progressive Scans (TOPS) mode, a new multi-channel single phase center multiple beam (SPCMB) TOPS mode is proposed in this paper for high-resolution wide-swath (HRWS) imaging. However, the progressive azimuth beam scanning leads to the Doppler spectrum aliasing and both beam center time and Doppler centroid varying with the target's azimuth location. Challenges may arise for processing the SPCMB-TOPS SAR data from these problems. In this paper, an efficient full aperture imaging approach is proposed to process the raw data. The sketch of the proposed imaging approach is described in detail. Simulation results of point targets validate the proposed imaging approach.

1. INTRODUCTION

The Synthetic Aperture Radar (SAR) is an all-weather imaging tool that achieves fine along-track resolution by taking the advantage of radar motion to synthesize a large antenna aperture [1–6]. TOPS (Terrain Observation by Progressive Scans) [7] is a novel spaceborne SAR imaging mode which can be used to obtain wide swath coverage exchanged by the coarser azimuth resolution. In such imaging scheme, the antenna beam should be steered in both azimuth and elevation to obtain the wide swath coverage. The progressive azimuth beam steering leads to that targets with different azimuth locations will be illuminated by the completed azimuth antenna pattern (AAP). Therefore, it will greatly reduce the major drawbacks in the burst

Received 6 March 2011, Accepted 18 May 2011, Scheduled 20 May 2011

* Corresponding author: Wei Xu (iecasxuwei@gmail.com).

mode such as the obvious scalloping effect, azimuth varying signal to noise ratio (SNR) and ambiguity to signal ratio (ASR). Because of its wide swath coverage imaging capacity and excellent system performances, the TOPS mode has been first implemented in the TerraSAR-X satellite and then will be used by the European Space Agency (ESA) Sentinel-1 SAR sensor in its interferomerometric wide swath mode instead of traditional ScanSAR [8, 9]. The TOPS mode may also be used in the next generation Chinese spaceborne SAR sensor for its wide swath imaging, and its airborne experiment of the TOPS mode has been successfully carried out.

However, unambiguous wide swath coverage and high azimuth resolution pose contradicting requirements on the design of spaceborne SAR systems [10–20]. The impaired azimuth resolution is the major bottleneck of the novel TOPS mode, as future remote sensing missions require both wide swath coverage and high geometric resolution. To overcome the inherent limitation in the conventional spaceborne SAR systems, several techniques have been proposed [15–20]. The considering multiple azimuth beam SAR systems allow an effective decrease in the desired pulse repetition frequency (PRF) or an improved azimuth resolution of a spaceborne SAR system, while the Doppler bandwidth is still adequately sampled. In this paper, we will introduce the technique of single phase center multiple azimuth beam (SPCMB) to improve the impaired azimuth resolution in the TOPS mode by extending azimuth beam interval.

In this paper, a novel spaceborne SPCMB-TOPS mode is proposed to achieve both wide swath coverage and high azimuth resolution. Afterwards, we focus on presenting an efficient imaging approach to process the SPCMB-TOPS mode raw data. To validate the proposed imaging approach, simulation experiments of point targets are carried out. This paper is arranged as follows. In Section 2, the TOPS mode and the SPCMB-SAR systems are reviewed. Afterwards, a novel spaceborne SPCMB-TOPS mode is proposed for high resolution wide swath (HRWS) imaging. In Section 3, the basic properties in azimuth of the SPCMB-TOPS SAR data are analyzed. The proposed imaging approach is described in detail in Section 4. In Section 5, some simulation results are given to validate the proprosed imaging approach. Some useful conclusions are reported in Section 6.

2. SPCMB-TOPS MODE

In this section, the novel TOPS mode and the SPCMB-SAR systems are reviewed. Afterwards, a novel SPCMB-TOPS mode is proposed to achieve both wide swath coverage and high azimuth resolution.

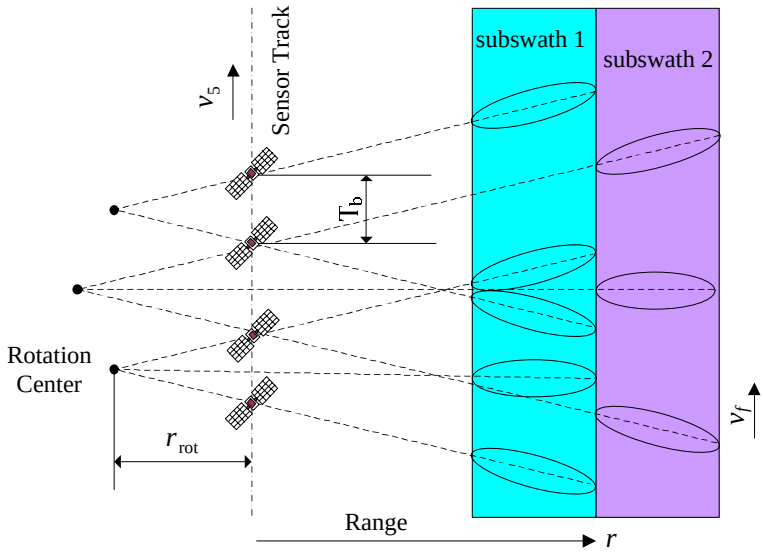

Figure 1. TOPS mode acquisition geometry.

2.1. TOPS Mode

In this paper, we consider the general TOPS mode with two subswaths geometry, as shown in Figure 1. The system requires the sensor antenna beam be steered in both elevation and azimuth. In elevation, the antenna beam scans cyclically from subswath to subswath by using the burst mode; in azimuth, the antenna beam is swept from aft to fore to shrink the illumination time but with the completed AAP illumination for each target. In Figure 1, t defines the slow time (in azimuth), v_s is the velocity of the satellite, ω_r is the azimuth beam rotation rate. By taking this rotation into account, echoes of each target are weighted by the reduced AAP. The new AAP can be regarded as [7]:

$$G_{\text{TOPS}}(t) \simeq G_0 \text{sinc}^2 \left[\frac{L_a}{\lambda} \frac{vt}{r} \left(1 + \frac{r\omega_r}{v} \right) \right] \tag{1}$$

where G_0 is a constant and represents the maximum gain of the AAP, L_a is the length of the antenna, v is the effective velocity of the SAR sensor in the imaging plane, r is the slant range. $G_{\text{TOPS}}(t)$ can be equivalent to the AAP of a fixed antenna in the stripmap mode, but shrunk by a factor A:

$$A(r) = 1 + \omega_r r / v \tag{2}$$

This factor shrinks the target illumination time and is responsible for the coarser azimuth resolution. Therefore, the TOPS mode achieves wide swath coverage but with an azimuth resolution A times coarser than the stripmap mode with the same antenna length. However, the azimuth beam steering scheme makes echoes of targets with different azimuth locations are weighted by the completed AAP. Therefore, compared with conventional ScanSAR, obvious scalloping effect, azimuth varying SNR and ASR in the burst mode will be seriously reduced.

2.2. Multi-Channel SPCMB-SAR System

The operation scheme of the conventional SPCMB-SAR system [15] is to transmit pulses into a single broad azimuth beam and receive echoes on multiple narrow continuous azimuth beams which span the mainlobe width of the transmit beam as shown in Figure 2(a). In such imaging scheme, the raw data are spilt according to the azimuth angular position recorded in a separate azimuth receive channel, and the data in each channel is sampled at the Nyquist rate appropriate to the bandwidth of the narrow receive beam. Therefore, this technique can overcome the inherent limitation in the conventional one-channel SAR system. However, the major drawback of such operation scheme

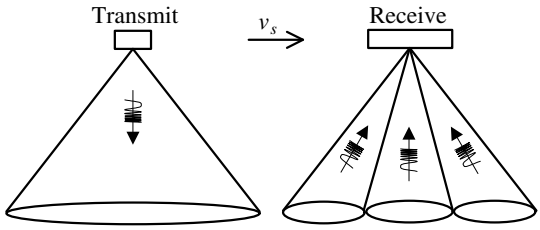

(a) Conventional SPCMB-SAR system

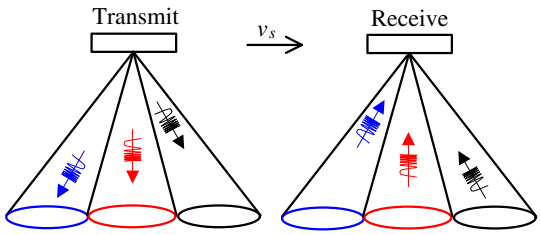

(b) Modified SPCMB-SAR system

Figure 2. Single phase center multiple beam (SPCMB) SAR system.

is the increased azimuth ambiguous energy due to the overlap between the mainlobe of the receive beam and the sidelobes of its adjacent receive beams. To achieve the tolerant ambiguity level, the operated pulse repetition frequency (PRF) should be about 30% higher than the ideal case of without any overlap in azimuth [15, 16]. Therefore, the azimuth receive interbeam suppression is usually required to improve the system performances and make the system more viable.

One possible solution of this problem is that the broad azimuth transmit beam is also generated by the multiple narrow azimuth beams. Moreover, orthogonal signals with different waveform encoding are transmitted through the different azimuth beams for the interbeam ambiguity suppression. However, this approach is effective in the case of isolated point targets, as the mere use of the orthogonal waveforms only disperse ambiguous energy not indeed suppress the ambiguous energy [17]. Based on the relation between the side looking angel and the transmitted time delay, the transmitted pulse with a large duration is divided into multiple sub-pulses and sub-pulses with different time delays are transmitted by the different azimuth beams as shown in Figure 2(b). Afterwards, the interbeam suppression can be easily implemented by digital beamforming (DBF) on receive with the large receive antenna in elevation [19, 20].

In this paper, the modified SPCMB technique is introduced in the TOPS mode to improve the impaired azimuth resolution. Obviously, there are several advantages in the proposed SPCMB-TOPS mode. First, the TOPS mode achieves ultra wide swath coverage with the inconspicuous scalloping effect. Second, the impaired azimuth resolution in the TOPS mode is improved by introducing the modified SPCMB technique. Third, the extended azimuth beam width is obtained by multiple azimuth beams synthesis instead of the transmit antenna reduction, as the smart transmit antenna leads to the lower output signal-to-noise (SNR) ratio or the increased transmit power requirement to achieve the desired SNR. Finally, the novel scan-on-receive (SCORE) technique [16, 19, 20], which is usually adopted in the wide swath imaging mode for future spaceborne remote sensing missions to improve system performances, can implement the azimuth interbeam suppression to reduce the azimuth ambiguity level. Therefore, the proposed SPCMB-TOPS mode is a potential imaging scheme to obtain both wide swath coverage and high resolution for the next generation SAR missions.

3. SPCMB-TOPS SAR RAW DATA

In the TOPS mode, the azimuth beam is actively steered from aft to fore during the whole acquisition time, and the progressive azimuth beam scanning leads to a reduced Doppler bandwidth of point target. Moreover, the constant azimuth beam rotation rate ω_r in the TOPS mode introduces a constant Doppler centroid varying rate and a shrinking factor A as follows:

$$k_{rot} = \frac{2v\omega_r}{\lambda} = -\frac{2v^2}{\lambda r_{rot}} \tag{3}$$

$$A(r) = 1 + \frac{\omega_r \cdot r}{v} \tag{4}$$

where r_{rot} is the slant range from the SAR sensor to the virtual rotation center as shown in Figure 1, λ is the wavelength. Afterwards, the Doppler bandwidth B_d of the point target and the whole Doppler bandwidth B_b of a single burst in the TOPS mode are respectively given as follows:

$$B_d = B_f / A(r) \tag{5}$$

$$B_b = k_{rot} \cdot T_b + B_f > \text{PRF} \tag{6}$$

where T_b is the burst duration, and B_f is the azimuth beam bandwidth. As a result, the progressive azimuth beam steering leads to the whole Doppler bandwidth in each azimuth channel spanning over several PRF intervals. Moreover, with the multiple azimuth channels in the SPCMB-SAR systems, the whole Doppler bandwidth B_s in the SPCMB-TOPS SAR system is increased to:

$$B_s = k_{rot} \cdot T_b + N \cdot B_f \tag{7}$$

where N is the number of azimuth channels in the SPCMB-TOPS mode.

Taking the SPCMB-TOPS SAR system with two azimuth channels as an example, Figure 3 shows the time frequency diagram (TFD) of the SPCMB-TOPS mode SAR data in azimuth. For each azimuth channel, the PRF is just selected at the Nyquist rate appropriate to the bandwidth of the narrow azimuth beam. Moreover, both the azimuth beam center time and the target Doppler centroid vary with the target azimuth location, and challenges may arise for the azimuth bandwidth synthesis from the variant azimuth beam center time and the variant target Doppler centroid.

4. IMAGING APPROACH

According to the special characteristics of the SPCMB-TOPS raw data in the azimuth time-frequency domain, an efficient imaging approach

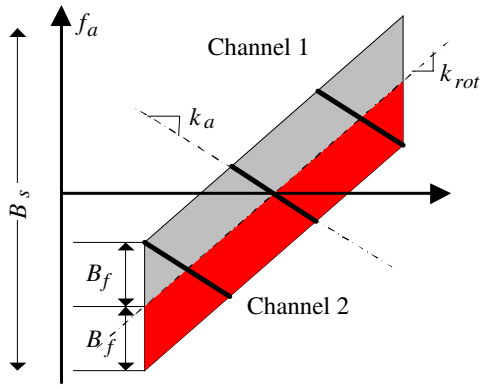

Figure 3. Time frequency diagram (TFD) of the SPCMB-TOPS data in azimuth.

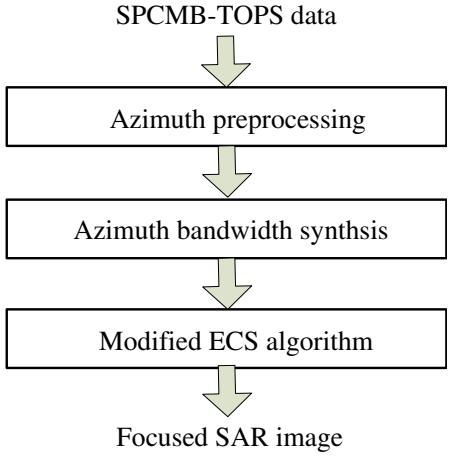

Figure 4. Block diagram of the proposed imaging approach.

is proposed as shown in Figure 4. This approach includes three major steps: azimuth preprocessing to resolve the aliased Doppler spectrum, azimuth bandwidth synthesis to improve the azimuth resolution and monostatic TOPS SAR imaging algorithm.

4.1. Azimuth Preprocessing

To resolve the aliased Doppler spectrum, this paper presents two efficient approaches. One is implemented by multiple azimuth data mosaicking, while the other is achieved by zero padding in the Doppler

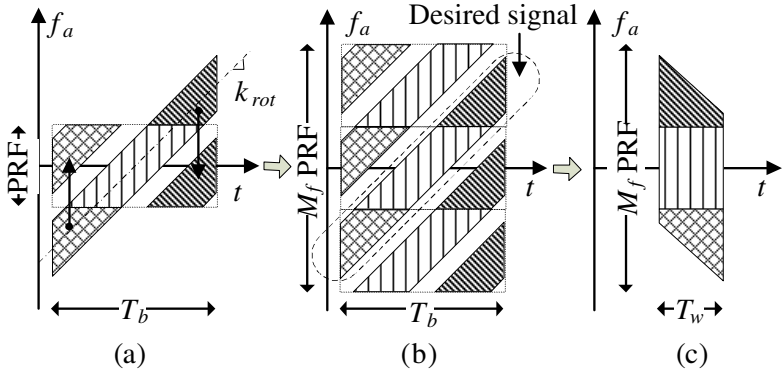

Figure 5. Azimuth data up-sampling by multiple data mosaicking.

domain.

The first approach to unfold the aliased Doppler spectrum is as shown in Figure 5 and summarized as follows:

(1) Fourier Transforming (FT) the SPCMB-TOPS raw data of each azimuth channel in azimuth. As the Doppler bandwidth B_b is much greater than the system PRF, the Doppler spectrum in each azimuth channel is aliased as shown in Figure 5(a).

(2) Mosaicking of M_f copies of the raw data in the Doppler domain as shown in Figure 5(b), the number M_f is as follows:

$$M_f = \left\lceil \frac{B_s}{\mathrm{PRF}} \right\rceil \tag{8}$$

where $\lceil \cdot \rceil$ is the "rounding to largest integer" operator.

(3) To obtain the desired azimuth signal, an azimuth scaling function $H_{DE}(f_a)$ is introduced as follows:

$$H_{DE}(f_a) = \exp\left[j\pi \frac{(f_a - f_{sdc,i})^2}{k_{rot}} \right] \tag{9}$$

where f_a is the Doppler frequency, and $f_{sdc,i}$ is the Doppler centroid in the ith azimuth channel. Afterwards, the new Doppler modulation rate k_{a1} is computed as:

$$k_{a1} = \left(\frac{1}{k_a} - \frac{1}{k_{rot}} \right)^{-1} = \frac{k_a \cdot k_{rot}}{k_{rot} - k_a} = \frac{A-1}{A} k_a \tag{10}$$

where $k_a = 2v^2/(\lambda r)$ is the Doppler frequency modulation rate. Afterwards, the azimuth varying azimuth beam center time is

removed and the effective signal duration is reduced from T_b to T:

$$T = \frac{B_d}{k_{a1}} = \frac{B_f}{A} \cdot \frac{A}{(A-1)k_a} = \frac{B_f}{k_{rot}} \tag{11}$$

It can be seen that the new effective signal duration doesn't depend on the target slant range.

(4) Azimuth Inverse Fourier Transforming (IFT) the raw data, and low-pass filtering the azimuth data in the azimuth time domain to obtain the desired signal. The duration of the low-pass filter T_w is as:

$$T_w = T \tag{12}$$

The second approach implemented by zero padding in the Doppler domain as shown in Figure 6 leads to the following steps:

(1) Removing azimuth varying target Doppler centroids by the reference de-rotation function g_{de}. The g_{de} is described as follows:

$$g_{de} = \exp\left[-j\pi k_{rot}(t - t_{mid})^2\right] \tag{13}$$

where t_{mid} is the center time of the burst. With this de-rotation function, the Doppler bandwidth of the imaged scene will be the same as the bandwidth of point target, and it can be computed as follows:

$$B_{d1} = \frac{(|k_a| + k_{rot}) \cdot B_d}{|k_a|} = A \cdot B_d = B_f < \text{PRF} \tag{14}$$

It can be seen that the whole Doppler spectrum aliasing problem will not exist after removing azimuth varying target Doppler centroids. After the azimuth FT operation, zero padding operation is taken in the range of $[-B_s/2, -\text{PRF}/2 + f_{sdc,i}]$ and $[\text{PRF}/2 + f_{sdc,i}, B_s/2]$ as shown in Figure 6(b), and the number of azimuth pixels is increased from $T_b \cdot \text{PRF}$ to $T_b \cdot B_s$.

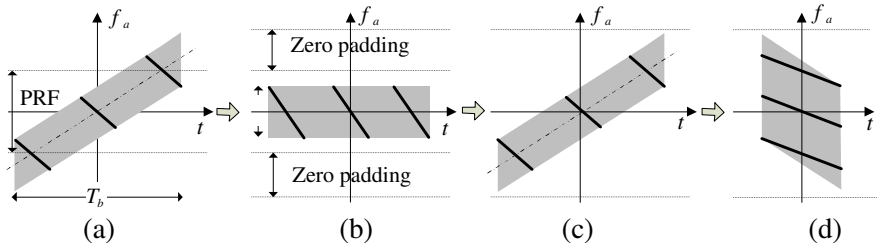

Figure 6. Azimuth data up-sampling by zero padding.

(2) As range cell migration correction (RCMC) is performed in the Doppler domain and depends on the target Doppler instantaneous frequency, azimuth varying target Doppler centroids should be recovered as shown in Figure 6(c) by the reference function g_{re} which is the conjugated function of g_{de}.

(3) Fourier Transforming the SPCMB-TOPS raw data, and removing azimuth varying beam center time by the reference deramping function $H_{DE}(f_a)$, similar to the third step of the first approach.

(4) Azimuth IFT the residual raw data, and low-pass filtering the azimuth data in the azimuth time domain as in the fourth step of the first unfolding approach.

4.2. Azimuth Bandwidth Synthesis

To improve the impaired azimuth resolution in the TOPS mode, azimuth bandwidths of multiple azimuth channels in the SPCMB-TOPS SAR system should be combined together. As the azimuth variant beam center time in the TOPS mode is removed in the azimuth preprocessing step, azimuth bandwidth synthesis in the SPCMB-TOPS mode can be easily implemented in the azimuth time domain. A block diagram of azimuth multi-channel data reconstruction in the SPCMB-TOPS SAR system with two azimuth channel is shown in Figure 7. To combine the azimuth multi-channel data together in the time domain, a short time delay $t_{c,i}$ for each azimuth channel should be implemented

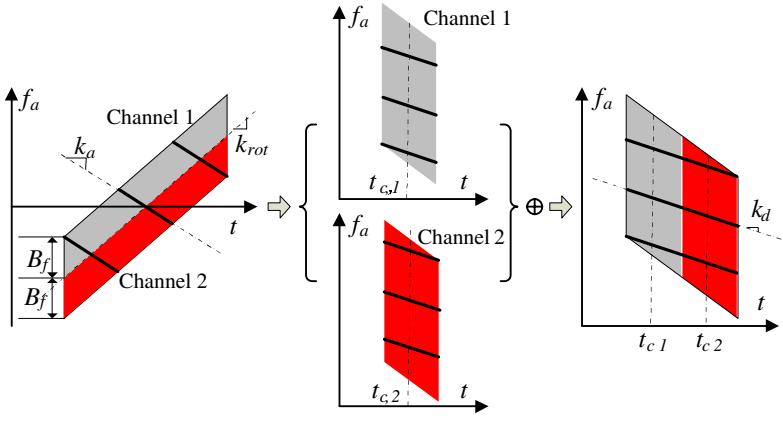

Figure 7. Azimuth bandwidth synthesis implemented in the time domain.

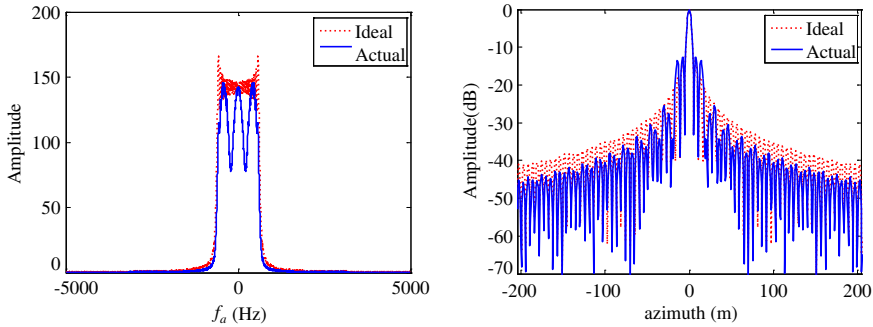

(a) Doppler bandwidth (b) Compression result

Figure 8. Results of azimuth bandwidth synthesis.

and given as follows:

$$t_{c,i} = t_{c,1} + (i-1) \cdot T \tag{15}$$

where $t_{c,1}$ is a constant, and $t_{c,1} = 0$ is assumed for simplicity in this paper. As the azimuth signal of the SAR raw data is weighted by the AAP, the synthetic azimuth spectrum undulation caused by the AAP of each narrow azimuth beam leads to imaging quality worsening as shown in Figure 8. Therefore, the gain reduction of each azimuth channel should be compensated, while azimuth bandwidth synthesis is performed in the azimuth time domain.

Different from azimuth data reconstruction algorithms in the Displaced Phase Center Multiple Beam (DPCMB) SAR systems in [21, 22], multiple linear filters for azimuth multi-channel data reconstruction are described as follows:

$$h_i(t) = \text{sinc}^{-2}\left(\frac{t - t_{c,i} - t_{mid}}{T}\right) \cdot \text{rect}\left(\frac{t - t_{c,i} - t_{mid}}{T}\right) \tag{16}$$

Finally, the filtered signals can be combined coherently, as shown in Figure 7.

4.3. Modified ECS Algorithm

After the above two processing steps, the TFD of the SPCMB-TOPS mode is quite similar to the TFD of ScanSAR. The Extended Chirp Scaling (ECS) algorithm [23] is an efficient imaging approach to process the ScanSAR data. However, it should be noted that the additional azimuth data extension is required to avoid wrap effect, while the hyperbolic azimuth phase history for all targets is removed and a constant linear frequency modulation for the whole subswath

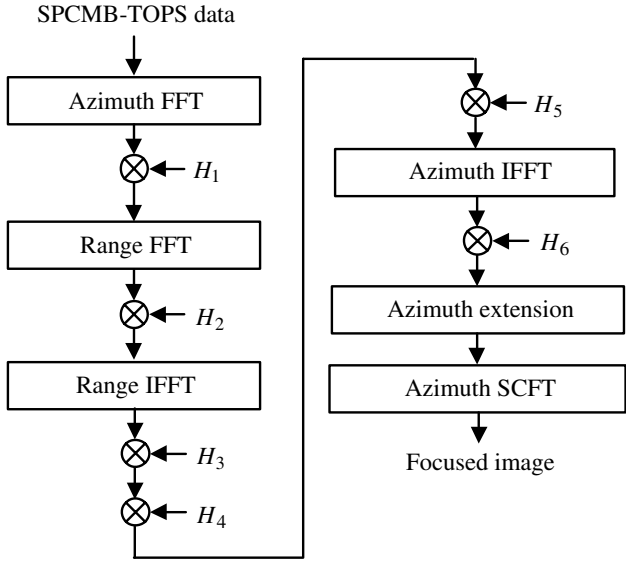

Figure 9. Block diagram of the proposed modified ECS algorithm.

is introduced. Moreover, the subswath width in the SPCMB-TOPS mode is much larger than conventional ScanSAR and its whole Doppler bandwidth is also much greater than conventional ScanSAR. Therefore, the additional azimuth data extension is much larger than ScanSAR. It seems that the classic ECS algorithm achieves the SPCMB-TOPS SAR data focusing not very efficiently.

This paper presents a modified ECS algorithm for the residual SPCMB-TOPS raw data. The block diagram of the modified ECS algorithm is shown in Figure 9. The transfer functions H_1, H_2, H_3 and H_4 in Figure 9 can be found in [23]. In [23], the hyperbolic azimuth phase history for all targets is removed and a constant linear frequency modulation for the whole subswath is introduced. However, the transfer function H_5 in this paper just removes the higher order terms, and it can be expressed as follows:

$$H_5 = \exp\left[j\frac{4\pi r}{\lambda}\left(\beta(f_a)-1\right)\right]\exp\left[j\pi\frac{\lambda r}{2v^2}f_a^2\right]\exp\left[j2\pi\cdot\Delta t\cdot f_a\right] \quad (17)$$

with

$$\beta(f_a) = \sqrt{1-\left(\frac{\lambda f_a}{2v}\right)^2} \quad (18)$$

$$\Delta t = \frac{\lambda f_{sdc}}{2v^2}\left[\frac{r-r_{rot}\beta(f_{sdc})}{\beta(f_{sdc})}-(r-r_{rot})\right] \quad (19)$$

where f_{sdc} is the Doppler centroid of the burst in the SPCMB-TOPS mode. After the above processing steps, the TOPS raw data in the range-Doppler domain can be expressed as follows:

$$\begin{aligned} sS(\tau, f_a) &= C \cdot K_r \tau_p \cdot \mathrm{sinc}\left[\pi K_r \tau_p \left(\tau - \frac{2r}{c}\right)\right] \exp\left[-j\frac{4\pi r}{\lambda}\right] \\ &\quad \times \exp\left[j\pi \frac{\lambda(r - r_{rot})}{2v^2} f_a^2 - j2\pi f_a \frac{x}{v} + j2\pi \cdot \Delta t \cdot f_a\right] \end{aligned} \quad (20)$$

where C is a constant, τ is the slow time, c is the light speed, x indicates the target azimuth location, K_r and τ_p denote the modulation rate and the pulse duration of the transmitted pulse, respectively. The deramping function H_6 is as follows:

$$H_6(t) = \exp\left[j\pi \frac{2v^2}{\lambda(r - r_{rot})} t^2\right] \exp\left[j2\pi \frac{2v^2}{\lambda(r - r_{rot})} \cdot \Delta t \cdot t\right] \quad (21)$$

If the conventional azimuth FT is carried out after multiplying H_6, the focused data can be expressed as:

$$\begin{aligned} sS_6(\tau, f_a) &= FT\{ss_5(\tau, t) \cdot H_6\} \\ &= C_1 \cdot \mathrm{sinc}\left[\pi K_r \tau_p \left(\tau - \frac{2r}{c}\right)\right] \\ &\quad \mathrm{sinc}\left[\pi \Delta t' \cdot N_{fft} \left(f_a - \frac{2v^2}{\lambda(r - r_{rot})} \cdot \frac{x}{v}\right)\right] \end{aligned} \quad (22)$$

where C_1 is a constant, $FT\{\cdot\}$ denotes the FT operator, and $ss_5(\tau, t)$ is the raw data of (20) in the two dimension (2D) time domain. As a result, the output azimuth sampling interval for each range bin is:

$$\Delta x = \frac{1}{\Delta t' \cdot N_{fft}} \cdot \frac{\lambda(r - r_{rot})}{2v} \quad (23)$$

where $\Delta t' = 1/\mathrm{PRF}$ is the azimuth sampling interval, and N_{fft} is the number of pixels used for the azimuth Fast Fourier Transform (FFT). Therefore, additional resampling for azimuth geometric correction is required. To avoid the additional resampling operation, the scaled Fourier transform (SCFT) is taken instead of the conventional FT operator. The kernel of the SCFT operation is given as follows:

$$h_{\mathrm{ker},az} = \exp\left[-j2\pi \frac{r_0}{r - r_{rot}} f_a t\right] \quad (24)$$

where r_0 is the selected range. After the SCFT operation, the focused

Table 1. System parameters.

Parameters	Value
Carrier frequency	9.65 GHz
Azimuth beam width	0.33°
Number of azimuth channels	3
System PRF	3475 Hz
Pulse duration	4 μs
Pulse bandwidth	100 MHz
Sampling frequency	120 MHz
Effective velocity	6800 m/s
Burst duration	0.48 s
Slant range of imaging center	600 km
Azimuth beam rotation rate	3.225°/s

signal is:

$$\begin{aligned} sS_6(\tau, f_a) &= \mathrm{SCFT}\{ss_5(\tau, t) \cdot H_6\} \\ &= C_2 \cdot \mathrm{sinc}\left[\pi K_r \tau_p \left(\tau - \frac{2r}{c}\right)\right] \\ &\quad \mathrm{sinc}\left[\pi \Delta t' \cdot N_{fft} \frac{r - r_{rot}}{r_0} \left(f_a - \frac{2v^2}{\lambda(r - r_{rot})} \cdot \frac{x}{v}\right)\right] \end{aligned} \quad (25)$$

Then, the output azimuth sampling interval for each range bin is:

$$\Delta x = \frac{1}{\Delta t' \cdot N_{fft}} \cdot \frac{\lambda r_0}{2v} \quad (26)$$

From (26), it can be seen that the uniform azimuth sampling interval for each range bin is obtained. The SCFT operation in the discrete domain is the chirp-z transform which can be efficiently performed by introducing the FFT codes [24].

5. SIMULATION EXPERIMENT

To validate the presented imaging scheme and the proposed efficient imaging algorithm, a simulation experiment about point targets is carried out. The parameters are listed in Table 1, and simulation results are obtained from Matlab.

The designed imaged scene including five point targets is shown in Figure 10, and P1 is located on the center of the designed scene. First, we put the designed scene on the border of the burst imaging

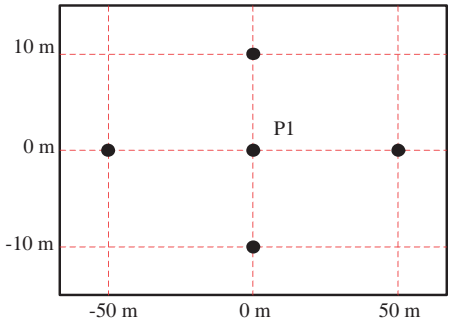

Figure 10. The designed imaged scene.

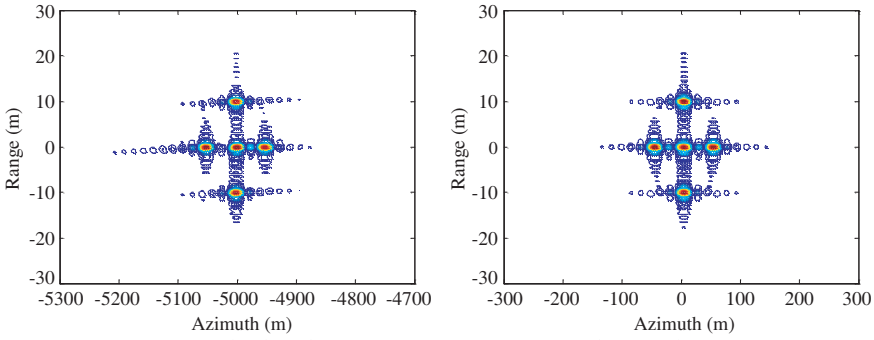

Figure 11. Imaging results in an azimuth channel.

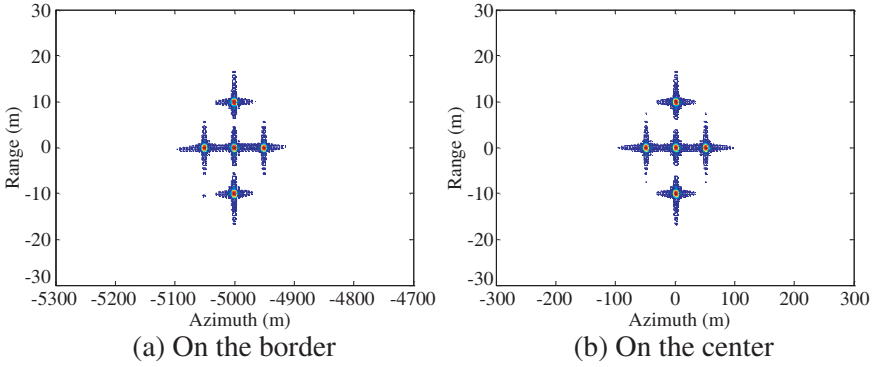

Figure 12. Imaging results after azimuth bandwidth synthesis.

Table 2. Results of point target P1 analysis in an azimuth channel.

	Range			Azimuth		
	Resolution	PSLR	ISLR	Resolution	PSLR	ISLR
On the border	1.33 m	−13.28 dB	−10.02 dB	14.34 m	−13.25 dB	−10.08 dB
On the center	1.33 m	−13.26 dB	−10.00 dB	14.32 m	−13.25 dB	−10.12 dB
Theory value	1.33 m	−13.26 dB	−9.80 dB	14.27 m	−13.26 dB	−9.80 dB

Table 3. Results of point target P1 analysis after azimuth bandwidth synthesis.

	Range			Azimuth		
	Resolution	PSLR	ISLR	Resolution	PSLR	ISLR
On the border	1.33 m	−13.27 dB	−9.98 dB	4.86 m	−13.23 dB	−9.68 dB
On the center	1.33 m	−13.26 dB	−10.01 dB	4.81 m	−13.26 dB	−9.81 dB
Theory value	1.33 m	−13.26 dB	−9.80 dB	4.76 m	−13.26 dB	−9.80 dB

scene in azimuth, while the relative azimuth range of point target P1 is 5 km. Its imaging result in a single azimuth channel is shown in Figure 11(a). Afterwards, the designed scene is located on the center of the burst imaging scene. Figure 11(b) shows its imaging result in a single azimuth channel. Both imaging results show the well focused features. Moreover, targets with different azimuth locations are illuminated with the different squint angles in the TOPS mode. From Figure 11, the limited squint angles can be obviously found.

To improve the impaired azimuth resolution in the TOPS mode, the Doppler bandwidths in all azimuth channels should be combined together. With the proposed imaging approach, Figure 12 shows the imaging results with the well focused features after azimuth bandwidth synthesis. Compared with imaging results in Figure 11, the obtained azimuth resolution in the SPCMB-TOPS mode is obviously improved.

The results of the measurements carried out on the point target P1 of Figures 11 and 12 are summarized and listed in Table 2 and Table 3. Moreover, the theoretical values of resolution, peak sidelobe ratio (PSLR) and integrated sidelobe ratio (ISLR) are listed in both tables.

6. CONCLUSION

The novel TOPS mode can be used to obtain wide swath coverage but at cost of the impaired azimuth resolution. In this paper, a novel SPCMB-TOPS mode for both wide swath coverage and high azimuth resolution is presented. However, challenges may arise to process the raw data of the proposed mode due to its special imaging scheme in azimuth. Based on the special TFD in azimuth, an efficient imaging approach for the SPCMB-TOPS mode SAR data is proposed in this paper. Besides resolving the aliased Doppler spectrum, the first azimuth preprocessing step in this algorithm removes the variant azimuth beam center time. Afterwards, azimuth data from multiple azimuth channels can be combined together coherently in the time domain. To avoid the large azimuth data extension, the final azimuth FT operator in the ECS algorithm [23] is replaced by the SCFT operator. Simulation results of point targets show the improved azimuth resolution in the SPCMB-TOPS mode and validate both the presented imaging scheme and the proposed imaging approach.

ACKNOWLEDGMENT

This work was supported by the Department of Spaceborne Microwave Remote Sensing, Institute of Electronics, Chinese Academy of Sciences (IECAS).

REFERENCES

1. Chan, Y. K. and V. C. Koo, "An introduction to synthetic aperture radar (SAR)," *Progress In Electromagnetics Research B*, Vol. 2, 27–60, 2008.
2. Angulo, L. D., S. G. Garcia, M. Fernandez Pantoja, C. Cobos Sanchez, and R. Gomez Martin, "Improving the SAR distribution in petri-dish cell cultures," *Journal of Electromagnetic Waves and Applications*, Vol. 24, No. 5–6, 815–826, 2010.
3. Lim, S. H., J. H. Han, S.-Y. Kim, and N.-H. Myung, "Azimuth beam pattern synthesis for airborne SAR system optimization," *Progress In Electromagneitcs Research*, Vol. 106, 295–309, 2010.
4. Chan, Y. K. and S. Y. Lim, "Synthetic aperture radar (SAR) signal generation," *Progress In Electromagnetics Research B*, Vol. 1, 269–290, 2008.
5. Li, C. and D.-Y. Zhu, "A residue-pairing algorithm for insar phase

unwrapping," *Progress In Electromagnetics Research*, Vol. 95, 341–354, 2009.

6. Sun, J., S. Mao, G. Wang, and W. Hong, "Extended exact transfer function algorithm for bistatic SAR of translational invariant case," *Progress In Electromagnetics Research*, Vol. 99, 89–108, 2009.
7. Zan, F. D. and A. M. Guarnieri, "TOPSAR: Terrain observation by progressive scans," *IEEE Trans. Geosci. Remote Sens.*, Vol. 44, No. 9, 2352–2360, Sep. 2006.
8. Meta, A., J. Mittermayer, P. Prats, R. Scheiber, and U. Steinbrecher, "TOPS imaging with TerraSAR-X: Mode design and perfomance analysis," *IEEE Trans. Geosci. Remote Sens.*, Vol. 48, No. 2, 759–769, Feb. 2010.
9. Prats. P., R. Scheiber, J. Mittermayer, A. Meta, and A. Moreira, "Processing of sliding spotlight and TOPS SAR data using baseband azimuth scaling," *IEEE Trans. Geosci. Remote Sens.*, Vol. 48, No. 2, 770–780, Feb. 2010.
10. Chua, M. Y. and V. C. Koo, "FPGA-based chirp generator for high resolution UAV SAR," *Progress In Electromagnetics Research*, Vol. 99, 71–88, 2009.
11. Sun, J., S. Mao, G. Wang, and W. Hong, "Polar format algorithm for spotlight bistatic SAR with arbitrary geometry configuration," *Progress In Electromagnetics Research*, Vol. 103, 323–338, 2010.
12. Wei, S.-J., X.-L. Zhang, J. Shi, and G. Xiang, "Sparse reconstruction for SAR imaging based on compressed sensing," *Progress In Electromagnetics Research*, Vol. 109, 63–81, 2010.
13. Zhao, Y. W., M. Zhang, and H. Cheng, "An efficient ocean SAR raw signal simulation by employing fast Fourier transform," *Journal of Electromagnetic Waves and Applications*, Vol. 24, No. 16, 2273–2284, 2010.
14. Mao, X., D.-Y. Zhu, and Z.-D. Zhu, "Signatures of moving target in polar format spotlight SAR image," *Progress In Electromagnetics Research*, Vol. 92, 47–64, 2009.
15. Currie, A. and M. A. Brown, "Wide-swath SAR," *Proc. Inst. Electr. Eng. F — Radar Signal Process.*, Vol. 139, No. 2, 122–135, Apr. 1992.
16. Xu, W. and Y. Deng, "Multi-channel SAR system with reflector antenna for high-resolution wide-swath imaging," *IEEE Antenna and Wireless Propa. Lett.*, Vol. 9, 1123–1126, Dec. 2010.
17. Krieger, G., N. Gebert, and A. Moreira, "Multidimensional waveform encoding: A new digital beamforming technique for

synthetic aperture radar remote sensing," *IEEE Trans. Geosci. Remote Sens.*, Vol. 46, No. 1, 31–46, Jan. 2008.

18. Sun, B., J. Chen, C. S. Li, and Y. Q. Zhou, "Fa-Scansar: Full aperture scanning pulse by pulse for the nearspace slow moving platform borne SAR," *Progress In Electromagnetics Research B*, Vol. 25, 23–37, 2010.
19. Gebert, N., G. Krieger, and A. Moreira, "Multichannel azimuth processing in ScanSAR and TOPS mode operation," *IEEE Trans. Geosci. Remote Sens.*, Vol. 48, No. 7, 2994–3008, Jul. 2010.
20. Suess, M., B. Grafmueller, and R. Zahn, "A novel high resolution, wide swath SAR system," *Proc. IGARSS*, Sydney, Australia, 2001.
21. Krieger, G., N. Gebert, and A. Moreira, "Unambiguous SAR signal reconstruction from nonuniform displaced phase center sampling," *IEEE Geosci. Remote Sens. Lett.*, Vol. 1, No. 4, 60–264, Oct. 2004.
22. Gebert, N., G. Krieger, and A. Moreira, "Digital beamforming on receive: Techniques and optimization strategies for high-resolution wide-swath SAR imaging," *IEEE Trans. Aerosp. Electron. Syst.*, Vol. 54, No. 2, 564–592, Apr. 2009.
23. Moreira, A., J. Mittermayer, and R. Scheiber, "Extended chirp scaling algorithm for air- and spaceborne SAR data processing in stripmap and ScanSAR imaging modes," *IEEE Trans. Geosci. Remote Sens.*, Vol. 34, No. 5, 1123–1136, Sep. 1996.
24. Lanari, R., S. Hensley, and P. Rosen, "Chirp Z-transform based SPECAN approach for phase-preserving ScanSAR image generation," *Proc. Inst. Elect. Eng. — Radar Sonar Navig.*, Vol. 145, No. 5, 254–261, Oct. 1998.